

Robust Dynamical Decoupling Sequences for Individual Nuclear Spin Addressing

J. Casanova,* Z.-Y. Wang,[†] J. F. Haase,[‡] and M. B. Plenio[§]

Institut für Theoretische Physik, Albert-Einstein-Allee 11, Universität Ulm, D-89069 Ulm, Germany

We propose the use of non-equally spaced decoupling pulses for high-resolution selective addressing of nuclear spins by a quantum sensor. The analytical model of the basic operating principle is supplemented by detailed numerical studies that demonstrate the high degree of selectivity and the robustness against static and dynamic control field errors of this scheme. We exemplify our protocol with an NV center-based sensor to demonstrate that it enables the identification of individual nuclear spins that form part of a large spin ensemble.

I. INTRODUCTION

The quantum control and detection of individual constituents of nuclear spin ensembles represents a major technological challenge whose solution would enable the realization of robust large scale quantum registers that are required for quantum information processing as well as the observation of the structure and dynamics of biomolecules. The solution requires both the hardware of a physical sensor that is capable, in principle, of detecting the minute magnetic fields emanating from individual nuclear spins and the software, i.e. the control schemes and measurement protocols, that can isolate the signal of a target spin from both, the other nuclear spins in the ensemble and from environmental noise.

Recently, the exceptional properties of the nitrogen-vacancy (NV) center in diamond have led to rapidly growing interest into its use as a quantum device. Microwave radiation can manipulate coherently the electron spin of the NV center while its initialization and readout can be achieved optically [1, 2]. These tools enable the control of the hyperfine coupling of the NV center to nearby ¹³C nuclei to carry out their detection and polarization [3–7] as well as the realization of ¹³C-NV quantum gates [8, 9]. Furthermore, NV centers can be implanted close to the diamond surface where they can detect the signal of nuclear spins above the surface with single spin sensitivity [10] suggesting the possibility of examining the structure of biomolecules by means of carefully designed protocols [11–13].

These applications need to achieve simultaneously the decoupling from environmental noise while preserving the interaction with the object of interest. This can be achieved by dynamical decoupling (DD) protocols that refocus undesired couplings by means of control sequences that design filters [14–18] transmissive exclusively for very specific interactions and frequencies. As small errors in DD protocols can accumulate and exceed the environmental perturbation they are designed to protect against, robust schemes as exemplified by the CPMG [19, 20], the XY-family of pulses [21, 22] or concatenated DD [23] are highly desirable. Whereas these concepts are well understood for protecting single isolated qubits, their extension to multiple and interacting spins to address in-

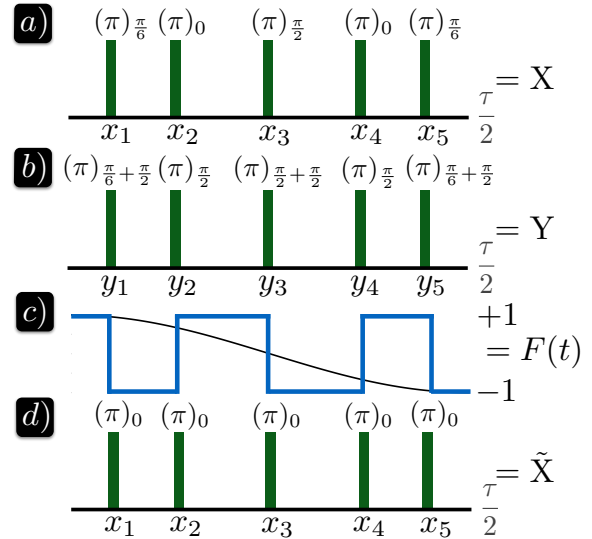


FIG. 1. (Color online) a) and b) Robust composite pulses with adaptable time variables x_i and y_i to increase the spectral resolution. Each bar corresponds to a π rotation around the axis defined by φ [denoted as $(\pi)_\varphi$]. The X, a), and Y, b), composite pulses will be connected in the robust AXY- n sequence. c) first Fourier component, a half-period, of the modulation function $F(t)$ for a composite pulse. A whole period τ corresponds to two successive X and (or) Y composite pulses. d) non-robust pulse unit \tilde{X} where all π rotations are applied in the same direction

dividual spins in an ensemble in the presence of environmental noise, remains an outstanding challenge.

Here we present a method for the tunable control and selective individual addressing of nuclear spins via the application of microwave radiation. Our protocol, denoted adaptive XY- n (AXY- n), based on non-equally spaced decoupling pulses [24], generates highly selective filter functions which ensures a precise discrimination of the magnetic response of external nuclear spins. We demonstrate the robustness of our method under realistic conditions including frequency detunings and amplitude fluctuations of the microwave driving. In this manner, our protocol represents a realistic procedure to achieve high-fidelity quantum gates between the quantum sensor and a spin cluster for quantum computing or quantum simulation purposes. At the same time, this proposal constitutes a highly selective detection method of different nuclear spins in the environment for structure determination with potential applications in biology as well as solid state physics.

* jcasanovamar@gmail.com

[†] zhenyu3cn@gmail.com

[‡] jan.haase@uni-ulm.de

[§] martin.plenio@uni-ulm.de

II. BASIC MODEL

In the presence of a strong magnetic field B_z , aligned with the NV axis \hat{z} , the Hamiltonian of the coupled NV center-nuclei system reads ($\hbar = 1$)

$$H = DS_z^2 - \gamma_e B_z S_z - \sum_j \gamma_j B_z I_j^z + S_z \sum_j \vec{A}_j \cdot \vec{I}_j + H_c. \quad (1)$$

Here $\gamma_{e,j}$ is the electronic, nuclear, gyromagnetic ratio and H_c describes the external microwave control fields. The interaction between NV center and nuclei is mediated by the hyperfine vector $\vec{A}_j = \frac{\mu_0 \gamma_e \gamma_j}{4\pi |\vec{r}_j|^3} [\hat{z} - 3 \frac{(\hat{z} \cdot \vec{r}_j) \vec{r}_j}{|\vec{r}_j|^2}]$, \vec{r}_j being the vector connecting the NV center and each nucleus in the environment. Due to the large zero field splitting $D = (2\pi)2.87$ GHz, we have eliminated non-secular components in Eq. (1). For the sake of clarity we neglect dipolar interactions between nuclei in our analytical work, but retain these interactions in our numerics. In the rotating frame of $DS_z^2 - \gamma_e B_z S_z$ and the control field H_c we obtain

$$H = - \sum_j \omega_j \hat{\omega}_j \cdot \vec{I}_j + \frac{m_s}{2} F(t) \sigma_z \sum_j \vec{A}_j \cdot \vec{I}_j. \quad (2)$$

Here, $\hat{\omega}_j$ is the unit vector of $\vec{\omega}_j = \gamma_j B_z \hat{z} - \frac{m_s}{2} \vec{A}_j$, $\omega_j = |\vec{\omega}_j|$ is the effective Larmor frequency, and $\sigma_z = |m_s\rangle\langle m_s| - |0\rangle\langle 0|$ the Pauli operator in the manifold of NV electron spin states $m_s = \pm 1$ and $m_s = 0$. For example, when the $m_s = 1$ electron spin state is chosen, a qubit between the $m_s = 1$ and $m_s = 0$ energy eigenstates is available while the $m_s = -1$ does not participate in the dynamics governed by Eq. (1).

The modulation function $F(t)$ takes the values $+1$ (-1) depending on whether an even (odd) number of π -pulses (instantaneous in our analytical model) have been applied, see Fig. 1. The appropriate tuning of $F(t)$ becomes crucial for accurate spin detection and control. We assume periodic pulse sequences, $F(t) = F(t + \tau)$ so that $F(t) = \sum_{k=0}^{\infty} f_k \cos(k\omega_{DD}t)$, where $\omega_{DD} = 2\pi/\tau$ and the Fourier coefficients are $f_k = \frac{2}{\tau} \int_0^{\tau} F(t) \cos(k\omega_{DD}t) dt$. The number of pulses and the spacing between them control $F(t)$ and therefore the values of the f_k . For example, CPMG sequences with pulse interval $\tau/2$ have only two pulses in a DD period τ , resulting in Fourier coefficients $f_0 = 0$ and $f_k = 4(k\pi)^{-1} \sin(\frac{k\pi}{2})$ for $k > 0$.

As the interaction between nuclei and sensor is governed by the second term of Eq. (2), it is convenient to move to a rotating frame w.r.t. $-\sum_j \omega_j \hat{\omega}_j \cdot \vec{I}_j$. We get

$$H_{\text{int}} = m_s F(t) \frac{\sigma_z}{2} \sum_j \vec{I}_j \cdot \vec{A}_j(t), \quad (3)$$

where $\vec{A}_j(t) = \vec{a}_j \cos(\omega_j t) + \vec{A}_j \times \hat{\omega}_j \sin(\omega_j t) + \vec{A}_j \cdot \hat{\omega}_j \hat{\omega}_j$ with $\vec{a}_j \equiv \vec{A}_j - \vec{A}_j \cdot \hat{\omega}_j \hat{\omega}_j$. Now we neglect the last two terms in $\vec{A}_j(t)$ because $F(t)$ is symmetric and oscillates with zero mean. Additionally we eliminate the counter rotating terms of H_{int} finding

$$H_{\text{int}} = m_s \frac{\sigma_z}{8} \sum_k f_k \sum_j \vec{I}_j \cdot \vec{a}_j [e^{i(\omega_j - k\omega_{DD})t} + \text{c.c.}]. \quad (4)$$

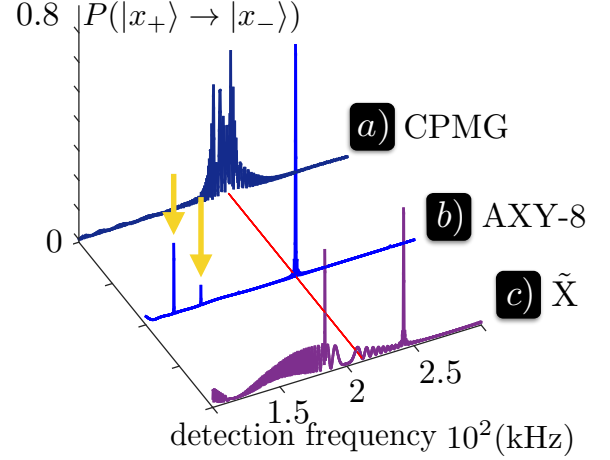


FIG. 2. (Color online) Sensor response (transition probability of an NV center coupled to a single nuclear spin) for different pulse sequences. The total evolution time is around 1.4 ms, $B_z = 200$ G, and microwave π -pulses with a duration of 12.5 ns are applied. A detuning of $\Delta = 1$ MHz and a microwave amplitude mismatch of 5% have been included. a) response for a CPMG sequence (600 pulses). b) uses the AXY-8 sequence, while in c) each X, or Y is replaced by the \tilde{X} composite pulse. The patterns in b) and c) are the result of the application of 3040 decoupling pulses with an interpulse spacing such that $f_{1DD} = \frac{1}{10} \frac{4}{\pi}$ and $f_2 = f_3 = f_4 = 0$. In b) we denote, with arrows, the location of spurious resonances, see the main text. The red line crossing the figure denotes the location of the resonance frequency.

In the following we identify the conditions that allow to tune the control field in order to address selectively the n -th spin. When the k_{DD} -th harmonic matches the Larmor frequency, $k_{DD}\omega_{DD} = \omega_n$, we have

$$H_{\text{int}} = \frac{m_s \sigma_z}{4} f_{k_{DD}} \vec{I}_n \cdot \vec{a}_n + \frac{m_s \sigma_z}{8} \sum_{j \neq n} f_{k_{DD}} \vec{I}_j \cdot \vec{a}_j [e^{i(\omega_j - \omega_n)t} + \text{c.c.}] + \frac{m_s \sigma_z}{8} \sum_{k \neq k_{DD}} \sum_j f_k \vec{I}_j \cdot \vec{a}_j [e^{i(\omega_j - k\omega_{DD})t} + \text{c.c.}]. \quad (5)$$

For a sufficiently strong magnetic field $\omega_j \sim \gamma_j B_z \gg |\vec{A}_j|$ the last line in Eq. (5) can be ignored if

$$|\gamma_j B_z| \gg k_{DD} |\vec{a}_j|. \quad (6)$$

Similarly, the second line in Eq. (5) is eliminated if

$$|\omega_j - \omega_n| \gg |f_{k_{DD}}| |\vec{a}_j|. \quad (7)$$

For sequences such as CPMG, XY-type, the Knill DD [25, 26], and their combinations [27, 28] where decoupling pulses are equally spaced, the coefficient $f_{k_{DD}} = 4 \sin(\frac{k_{DD}\pi}{2}) / (k_{DD}\pi)$ is not tunable and the strong interactions \vec{a}_j limit the addressability because of Eq. (7). Additionally, Eq. (6) limits the largest possible k_{DD} .

Now we will show how our approach can achieve arbitrary tuning of the value of the coefficient $f_{k_{DD}}$ to obtain the effective

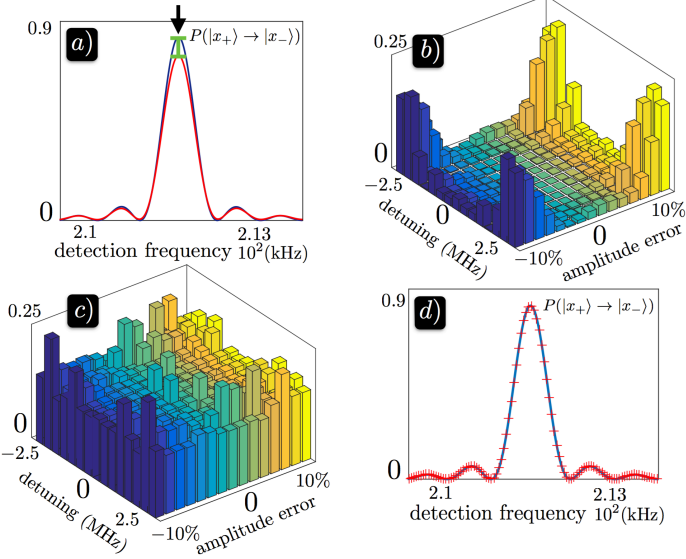


FIG. 3. (Color online) Difference between ideal and error-included patterns. a) quantity used for comparing the behavior of distinct sequences in the presence of errors - the difference between transition probabilities, see arrow, averaged over the frequency interval of the figure. In b), c), the difference for the sequences used in Figs. 2 b), c), is obtained for different values of the detuning and amplitude error. d) shows the patterns without (solid line) and with (red crosses) time-dependent microwave fluctuation in the control field.

Hamiltonian

$$H_{\text{int}} = \frac{m_s}{4} f_{k_{DD}} \sigma_z \vec{I}_n \cdot \vec{d}_n, \quad (8)$$

and therefore individual control of nuclear spins without the necessity of using high harmonics, i.e. large values of k_{DD} .

III. SHAPING THE FILTER FUNCTIONS

Since f_k depends on the overlap between $F(t)$ and each harmonic component, see Fig. 1 c), we can select sequences that tune f_k at will. Figs. 1 a) and b) present an example of our proposed pulse scheme where each X or Y composite pulse is made of 5 π -rotations applied along different directions for enhanced robustness. When equally spaced, X and Y converge to the Knill composite pulse used in the literature [25]. Every period τ includes two composite pulses X and Y that are applied time symmetric around the midpoint of the period but are otherwise arbitrary. This guarantees the even character of the Fourier expansion of $F(t)$. Accordingly, we have 5 controllable relative time variables x_j , or y_j , each of them measuring the relative positions of the first 5 pulses (applied at $0 < x_j \tau < \frac{\tau}{2}$). We can use these 5 variables to achieve $f_0 = 0$, and $f_{k_j} = 0$ with $j = 1, 2, 3$ and a tunable coupling constant for the k th harmonic $f_k = f_{k_{DD}}$. For example, one can adjust the interpulse spacing in such a way that $f_0 = f_2 = f_3 = f_4 = 0$ and $f_1 \neq 0$, meaning $k'_1 = 2, k'_1 = 3, k'_1 = 4$ and $k_{DD} = 1$.

We note that the symmetric construction $x_3 = \frac{1}{4}, x_4 = \frac{1}{2} - x_2$, and $x_5 = \frac{1}{2} - x_1$ [see Figs. 1 a) and 1 b)] enhances

robustness because it is able to cancel first and second order error contributions. This allows to extend our protocol to several thousands of imperfect decoupling pulses, see Appendix. The symmetric construction yields

$$f_k = \frac{4}{\pi k} \left\{ \sum_{j=1,2} (-1)^j [(-1)^k - 1] \sin(2\pi k x_j) + \sin\left(k \frac{\pi}{2}\right) \right\}, \quad (9)$$

which vanishes for even k . As an example we choose $f_3 = 0$ and $f_1 = f_{k_{DD}} \equiv f_{1_{DD}}$, and a solution is

$$x_{1,2} = \frac{1}{2\pi} \arctan \frac{\pm(3f_{1_{DD}}\pi - 12)w_1 + \sqrt{3}w_2}{\sqrt{6}\sqrt{w_2 - 96f_{1_{DD}}w_1\pi \pm w_1^2}\sqrt{3}w_2} \quad (10)$$

with the functions $w_1 = 4 - f_{1_{DD}}\pi$ and $w_2 = w_1[960 - 144f_{1_{DD}}\pi - 12(f_{1_{DD}}\pi)^2 + (f_{1_{DD}}\pi)^3]$. Here any $f_{1_{DD}}\pi \in (-8 \cos \frac{\pi}{9} + 4, 8 \cos \frac{\pi}{9} - 4)$ is possible. Note that for $f_{1_{DD}} \approx 0.16$, the solution $x_{1,2}$ reproduces the 5-pulse repetition unit in [29] (where all π rotations are applied about the same axis) which is designed for identifying coupled nuclei in a weak field regime *and* a semiclassical picture which can deviate from a full quantum description [30, 31]. For equally spaced pulses AXY- n converges to the $\text{KDD}_\phi - \text{KDD}_{\phi+\frac{\pi}{2}}$ sequences which are robust against imperfect pulses [26–28]. Additionally, we can use higher harmonics, $k_{DD} > 1$, to reduce the pulse number or to increase the total evolution time at a given magnetic field. For $f_1 = 0$ and $f_3 = f_{3_{DD}}$, we obtain

$$x_j = \frac{1}{4} - \frac{1}{2\pi} \arctan \sqrt{q_j^2 - 1}, \quad (11)$$

with $q_j = 4/[\sqrt{5 + \pi f_{3_{DD}}} + (-1)^j]$ and $j = 1, 2$, and $f_{3_{DD}} \in (-\frac{4}{\pi}, \frac{4}{\pi})$.

IV. ROBUSTNESS AGAINST ERRORS

In Fig. 2 we compare the transition probability between the $|x_\pm\rangle = \frac{1}{\sqrt{2}}(|0\rangle \pm |1\rangle)$ NV states for different decoupling sequences. Possible error sources are included in the control Hamiltonian

$$H_c = \Omega(t) \cos[(\omega_{NV} + \Delta)t][S_x \cos \varphi(t) + S_y \sin \varphi(t)], \quad (12)$$

where ω_{NV} is the resonant frequency of the NV transition, and the microwave pulses are imperfect, with a detuning error $\Delta = 1\text{MHz}$ and a 5% of error in the Rabi frequency $\Omega(t)$. The detuning error Δ takes into account the energy of the nitrogen spin intrinsic to the NV center. Because both the magnetic field and the hyperfine field \vec{A}_j for the nitrogen spin are oriented along the NV symmetry axis, flipping of the nitrogen spin can be neglected by secular approximation. When the intrinsic nitrogen spin is polarized, the detuning Δ can be made small by calibration. If the intrinsic nitrogen spin is not polarized, uncertainty of the nitrogen spin state introduce large energy shifts on the splitting between the NV states through the hyperfine interaction, and the unknown energy shifts cause

the detuning error within the range of about 1 MHz for naturally occurring ^{14}N spin [1, 32].

In Fig. 2 a) the resonance pattern for a CPMG sequence with $f_{1DD} = 4/\pi$ is plotted. Figs. 2 b) and c) show the result of a pulse sequence with $f_1 = f_{1DD} = \frac{1}{10}\frac{4}{\pi}$ and $f_2 = f_3 = f_4 = 0$. While the spectrum in Fig. 2 a) is distorted because of accumulated errors, Fig. 2 b) shows a clear pattern obtained by the AXY-8 sequence (AXY- n for $n = 8$, i.e. XYXYXYXY), where the pulses are repeatedly applied according to the pattern of XY-8. This is a sequence containing 8 composite pulses, X or Y, where X and Y are designed according to the scheme in Figs. 1 a) and b) respectively. Our simulations extend to 3040 pulses corresponding to a final evolution time ≈ 1.4 ms. We observe that the resonant peak is very sharp which is of considerable benefit for the filtering of noisy signals. Note that common to all pulsed schemes are spurious resonances due to the finite width of the microwave π -pulses [32]. We would like to stress however that the composite pulse structure of the AXY-8 sequence produces very narrow spurious peaks which, additionally, are far away from the principal resonance even in the presence of noise and imperfections (see Fig. 2 b)). Fig. 2 c) has been computed repeating the \tilde{X} sequence, see Fig. 1 d), where all π rotations are applied along the same axis. We can observe how the accumulated errors distort the pattern destroying any readable signal.

To investigate the behavior of each multipulse sequence in presence of strong error sources we compare the different patterns that appear when changing the conditions in H_c . In Fig. 3 a) the cases for $\Delta = 0$ and perfect microwave pulses (blue line), and $\Delta = 1$ MHz and a 10% of error in the rotating Rabi frequency (red line) for the the AXY-8 sequence are plotted. In Figs. 3 b) and c) we show the average difference between the transition probabilities in the ideal case and in the presence of error sources in a region close to the resonance position. The difference between patterns is small for AXY-8 in a detuning range of ± 1.5 MHz and $\pm 10\%$ in the microwave driving error, see Fig. 3 b). In the case of the combined sequence \tilde{X} , Fig. 3 c), the pulse errors rapidly accumulates. In this manner we confirm that the AXY-8 sequence is robust against realistic error sources allowing, at the same time, to accurately filter specific frequency-components.

Our AXY-8 is also robust against amplitude fluctuations in the driving field. In Fig. 3 d) we compare the result with (red crosses) and without (solid line) fluctuations in the control field. Fluctuations are modeled by an Ornstein-Uhlenbeck processes where the amplitude fluctuation $\Delta\Omega(t)$ evolves according to $\Delta\Omega(t + \Delta t) = \Delta\Omega(t)e^{-\Delta t/\tau_{mw}} + n_G \sqrt{\frac{c_{mw}\tau_{mw}}{2}}(1 - e^{-2\Delta t/\tau_{mw}})$ [33], $\tau_{mw} \approx 1$ ms being the correlation time of the microwave noise and $c_{mw} \approx 2\delta_\Omega^2\Omega^2\tau_{mw}^{-1}$ with the relative amplitude fluctuation $\delta_\Omega \approx 7 \times 10^{-3}$, see Ref [23]. Fig. 3 d) demonstrates that the effect of microwave fluctuations is negligible in the resonance pattern which confirms the robustness of our protocol.

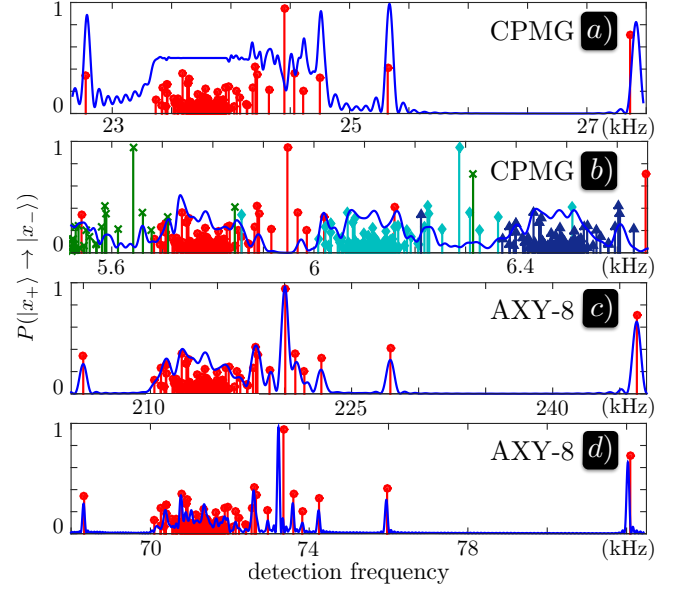


FIG. 4. a) (Color online) Resonance pattern for a CPMG sequence, 9^{th} harmonic used. The position of the vertical lines denote ω_j/k and their height denotes the strength of interaction between the sensor and the nucleus. In b) we can observe the effect of the overlap caused by $k = 35$ (diamonds), 33 (triangles), and 39 (crosses) harmonics on the spectrum of the $k = 37$ (circles) harmonic. c) and d) show resonance pattern in the AXY-8 sequence for the 1^{st} and 3^{rd} harmonics respectively. In each plot, the horizontal axis corresponds to the frequency range of the modulation function one should explore in order to obtain the nuclear response in the appropriate harmonic.

V. SINGLE SPIN ADDRESSING

Finally, we have performed simulations in a diamond containing 736 ^{13}C spins which are generated on random lattice sites of the diamond structure according to the natural abundance of 1.1% and $B_z = 200\text{G}$. In the simulation we use instantaneous pulses and a disjoint cluster expansion including dipolar interactions up to a group size of six ^{13}C [34]. In Figs. 4 a) and b) the patterns were obtained by CPMG sequences with a total evolution time ~ 1.4 ms. Fig. 4 a) shows the result for the 9^{th} harmonic of the 66-pulse CPMG sequence. In this sample, working at higher harmonics causes spectral overlap and difficulty in distinguishing signals. This can be observed in Fig. 4 b) where the 37^{th} harmonic (hence 16 pulses) has been used. Using the AXY-8 sequence, for the first [Fig. 4 c)] and third [Fig. 4 d)] harmonic, more spins can be resolved by individual resonant peaks. The sequence in Fig. 4 c) has been tuned to $f_{1DD} = \frac{4}{37\pi}$ and $f_k = 0$, k being 3 or any even number, and it uses 3000 decoupling pulses to obtain a total time duration equaling that of Figs. 4 a) and b). In Fig. 4 d), the third harmonic version with $f_{3DD} = \frac{4}{111\pi}$ and $f_k = 0$, k being 1 or any even number, can provide 3-fold evolution time (i.e., 4.2 ms) compared to the first harmonic version and hence narrower signal peaks. In both cases the resolution is increased in a way that permits individual addressing of a considerable number of spins without the prob-

lem of spectral overlaps.

VI. CONCLUSIONS

We have presented a protocol that allows for individual addressing of nuclear spins even in large assemblies and when weakly coupled to a sensor. Based on the application of non-uniformly spaced decoupling pulses our method obviates the need for high harmonics which reduces significantly peak pollution and consequently enhances both resolution and robustness. The method is generic as it permits the high-resolution detection of arbitrary magnetic moments by means of a quantum sensor. This scheme promises applications in the control of mesoscopic nuclear spin based quantum registers in diamond as well as the precise nuclear positioning in external probes including biomolecules.

VII. ACKNOWLEDGEMENTS

This work was supported by the Alexander von Humboldt Foundation, the ERC Synergy grant BioQ, the EU projects DIADEMS, SIQS and EQUAM as well as the DFG SFB TRR/21.

J. C. and Z.-Y. W. contributed equally to this work.

VIII. APPENDIX: ROBUSTNESS OF SYMMETRIC AX-Y-8

A. Control errors

To show the robustness of our protocol for leading and second order error contributions on the electron spin rotations it is sufficient to consider the pulse Hamiltonian

$$H = \Delta \frac{\sigma_z}{2} + \Omega(t) \frac{\sigma_{\phi(t)}}{2},$$

where Δ is a detuning, $\Omega(t) = \Omega$ during the pulse control and $\Omega(t) = 0$ between pulses. The phase $\phi(t)$ of the Pauli operator

$$\sigma_{\phi} \equiv \cos \phi \sigma_x + \sin \phi \sigma_y, \quad (13)$$

switches for different pulses. One can demonstrate that, up to second order on small parameters $\epsilon = \frac{\Delta}{\Omega}$ and δ , the latter being the microwave amplitude mismatch, the propagator associated to the imperfect rotation is

$$R_{\phi} = e^{-i \frac{(\pi-2\delta)}{\Omega} H} \approx -i \left(1 - \frac{\delta^2 + \epsilon^2}{2} \right) \sigma_{\phi} - i \epsilon \sigma_z + \left(\delta - \frac{\epsilon^2 \pi}{4} \right) \mathbb{I}. \quad (14)$$

Note that the small quantities δ and ϵ can be always written as $\delta = \eta \tilde{\delta}$ and $\epsilon = \eta \tilde{\epsilon}$ with $\eta < 1$, therefore we can make the expansion in terms of the η parameter.

B. Robust composite pulses

1. No pulse delay

The simplest case is that the pulses are applied subsequently without delay. A sequence of composite pulses for the X pulse has the propagator (without pulse delays) $X = R_{\frac{\pi}{6}} R_0 R_{\frac{\pi}{2}} R_0 R_{\frac{\pi}{6}}$. Using Eq. (14) and keeping up to the leading order (first order) of errors we find $X = O_0 + O(\eta^2)$, where

$$O_0 = i \sigma_x e^{-i \frac{\sigma_z \pi}{2}}, \quad (15)$$

is the perfect rotation for the X composite pulse. Therefore the X composite pulse cancels the leading order error.

2. Including pulse delay

We include pulse delays t_i between the $(i-1)$ -th and i -th pulses. In the interpulse spacing, the presence of the detuning Δ cannot be neglected because the accumulated effect Δt_i is not small for long pulse delays. With the pulse delays, the propagator of the imperfect composite X pulse is

$$X = U_{\frac{\pi}{6} \Delta_5} U_{0 \Delta_4} U_{\frac{\pi}{2} \Delta_3} U_{0 \Delta_2} U_{\frac{\pi}{6} \Delta_1}, \quad (16)$$

where

$$\begin{aligned} \Delta_1 &\equiv 2\Delta(t_1), \\ \Delta_2 &\equiv 2\Delta(t_2 - t_1), \\ \Delta_3 &\equiv 2\Delta(t_3 + t_1 - t_2), \\ \Delta_4 &\equiv 2\Delta(t_4 + t_2 - t_3 - t_1), \\ \Delta_5 &\equiv 2\Delta(t_5 + t_3 + t_1 - t_4 - t_2), \end{aligned} \quad (17)$$

and

$$U_{\phi, \Delta_i} = i(\eta^2 \tilde{\alpha}^2 - 1) \sigma_{\phi} - i \eta \tilde{\epsilon} \sigma_z U_{\Delta_i} + \eta \tilde{\delta} U_{\Delta_i} - \eta^2 \tilde{\beta}^2 U_{\Delta_i}, \quad (18)$$

with $\tilde{\alpha}^2 = \frac{\delta^2 + \epsilon^2}{2}$, $\tilde{\beta}^2 = \frac{\epsilon^2 \pi}{4}$, and $U_{\Delta_i} = e^{-i \Delta_i \sigma_z}$. The imperfect composite Y pulse is related with X pulse by

$$Y = U_z(\pi/2) X U_z^{\dagger}(\pi/2), \quad (19)$$

with $U_z(\pi/2) = e^{-i \frac{\sigma_z \pi}{2}}$. Now Eq. (16) can be expanded in different orders in η . For symmetric sequences we have

$$\begin{aligned} \Delta_4 + \Delta_5 &= \Delta_2 + \Delta_1, \\ \Delta_4 &= \Delta_2, \\ \Delta_5 &= \Delta_1. \end{aligned} \quad (20)$$

One can obtain the first order correction

$$O_1 = \eta(i \tilde{\epsilon} \sigma_z - \tilde{\delta})(U_{\Delta_1} - U_{\Delta_3}). \quad (21)$$

When the pulses are equally spaced we have $t_3 = t_2$ which according to Eqs. (17) implies $\Delta_1 = \Delta_3$ and therefore $U_{\Delta_1} - U_{\Delta_3} = 0$ which leads to $O_1 = 0$. To suppress higher order errors we will combine the composite X and Y pulses in XY sequences. Additionally we will demonstrate that even when the pulses on the inner level of the X or Y sequences are not equidistant but distributed according to Eq. (20) the errors up to second order in η can be cancelled.

3. AXY-4 sequence

When $\Delta_1 \neq \Delta_3$, that is the pulses are not equally spaced, $O_1 \neq 0$. Now we show how leading order error cancellation appear because the combination of the composite X and Y pulses, Eqs. (16) and (19), in the XY-4 configuration (this scheme constitutes the AXY-4 sequence). Up to the first order in η we have

$$X = O_0 + O_1, \quad (22)$$

$$Y = U_z(\pi/2)(O_0 + O_1)U_z^\dagger(\pi/2), \quad (23)$$

Now, by simply calculating the first order contribution in η to AXY-4 sequences (here XYXY, or YXYX) we have that for the XYXY sequence that term is

$$O_0 O_0^z (O_0 O_1^z + O_1 O_0^z) + (O_0 O_1^z + O_1 O_0^z) O_0 O_0^z = 0, \quad (24)$$

while for the YXYX reads

$$O_0^z O_0 (O_0^z O_1 + O_1^z O_0) + (O_0^z O_1 + O_1^z O_0) O_0^z O_0 = 0, \quad (25)$$

where $O_j^z = U_z(\pi/2)O_j U_z^\dagger(\pi/2)$. This means that terms going with η are cancelled because of the XYXY, or YXYX, construction. However, one can demonstrate that this cancellation does not require the application of the conditions in Eq. (20).

4. AXY-8 sequence

The symmetry imposed by our protocol, i.e. the conditions in Eq. (20), allows us to eliminate the second-order error contribution when we combine our composite pulse with the XY-8 sequence, namely, the AXY-8 protocol is applied. Note that to cancel the second-order error symmetric composite pulses are required. Non-symmetric composite pulse only eliminate the the leading order error because of the reasons explained in

the previous subsection. To make the argument complete let us additionally introduce second order error contributions in the discussion. This reads

$$\begin{aligned} O_2 = & -i\eta^2(\tilde{\epsilon}^2 + \tilde{\delta}^2)\left(\frac{3}{2}\sigma_{\frac{\pi}{6}}\sigma_y\sigma_{\frac{\pi}{6}} + \sigma_y\right) + \eta^2\tilde{\beta}^2(U_{\Delta_1} - U_{\Delta_3}) \\ & + i\eta^2(\tilde{\delta}^2 - \tilde{\epsilon}^2)(U_{\Delta_3+2}\sigma_{\frac{\pi}{6}}\sigma_x\sigma_{\frac{\pi}{6}} + \sigma_{\frac{\pi}{6}}\sigma_x\sigma_{\frac{\pi}{6}}U_{\Delta_3+2}) \\ & + 2\eta^2(\tilde{\epsilon}\tilde{\delta})(U_{\Delta_3+2}\sigma_{\frac{\pi}{6}}\sigma_x\sigma_z\sigma_{\frac{\pi}{6}} + \sigma_{\frac{\pi}{6}}\sigma_z\sigma_x\sigma_{\frac{\pi}{6}}U_{\Delta_3+2}) \\ & + i\eta^2(\tilde{\epsilon}^2 + \tilde{\delta}^2)(U_{\Delta_1-3}\sigma_{\frac{\pi}{6}} + \sigma_{\frac{\pi}{6}}U_{\Delta_1-3}). \end{aligned} \quad (26)$$

Therefore, up to the second order one can write

$$X = O_0 + O_1 + O_2, \quad (27)$$

$$Y = U_z(\pi/2)(O_0 + O_1 + O_2)U_z^\dagger(\pi/2). \quad (28)$$

Now under the symmetry conditions in Eq. (20) we have up to the second order of errors XYXYXYXYX = $(\tilde{f}_0 + \tilde{f}_2)(f_0 + f_2)$, where

$$\begin{aligned} \tilde{f}_0 &= O_0 O_0^z O_0 O_0^z, \\ f_0 &= O_0^z O_0 O_0^z O_0, \\ \tilde{f}_2 &= O_0 O_0^z (O_0 O_2^z + O_1 O_1^z + O_2 O_0^z) \\ &+ (O_0 O_2^z + O_1 O_1^z + O_2 O_0^z) O_0 O_0^z \\ &+ (O_0 O_1^z + O_1 O_0^z)(O_0 O_1^z + O_1 O_0^z), \\ f_2 &= O_0^z O_0 (O_0^z O_2 + O_1^z O_1 + O_2^z O_0) \\ &+ (O_0^z O_2 + O_1^z O_1 + O_2^z O_0) O_0^z O_0 \\ &+ (O_0^z O_1 + O_1^z O_0)(O_0^z O_1 + O_1^z O_0). \end{aligned} \quad (29)$$

It can be calculated that the errors up to the second order $\tilde{f}_0 f_2 + \tilde{f}_2 f_0 = 0$ is eliminated by the symmetric construction of the AXY-8 sequences. That is, we have the robust sequence

$$\text{AXY-8} = \text{XYXYXYXYX} = \mathbb{I} + O(\eta^3), \quad (30)$$

where we have used that the error-free control $\tilde{f}_0 f_0 = \mathbb{I}$.

-
- [1] M. W. Doherty, N. B. Manson, P. Delaney, F. Jelezko, J. Wrachtrup and L. C. L. Hollenberg, Phys. Reports **528**, 1 (2013).
 - [2] V. V. Dobrovitsky, G. D. Fuchs, A. L. Falk, C. Santory and D. D. Awschalom, Annu. Rev. Condens. Matter Phys. **4**, 23 (2013).
 - [3] S. Kolkowitz, Q. P. Unterreithmeier, S. D. Bennett, and M. D. Lukin, Phys. Rev. Lett. **109**, 137601 (2012).
 - [4] T. H. Taminiau, J. J. T. Wagenaar, T. van der Sar, F. Jelezko, V. V. Dobrovitski, and R. Hanson, Phys. Rev. Lett. **109**, 137602 (2012).
 - [5] N. Zhao, J. Honert, B. Schmid, M. Klas, J. Isoya, M. Markham, D. Twitchen, F. Jelezko, R.-B. Liu, H. Fedder, and J. Wrachtrup, Nat. Nanotechnol. **7**, 657 (2012).
 - [6] P. London, J. Scheuer, J.M. Cai, I. Schwarz, A. Retzker, M.B. Plenio, M. Katagiri, T. Teraji, S. Koizumi, J. Isoya, R. Fischer, L.P. McGuinness, B. Naydenov and F. Jelezko, Phys. Rev. Lett. **111**, 067601 (2013)
 - [7] V. V. Mkhitarian, F. Jelezko, and V. V. Dobrovitski, E-print arXiv:1503.06811.
 - [8] T. van der Sar, Z. H. Wang, M. S. Blok, H. Bernien, T. H. Taminiau, D. M. Toyli, D. A. Lidar, D. D. Awschalom, R. Hanson, and V. V. Dobrovitski, Nature **484**, 82 (2012).
 - [9] T. H. Taminiau, J. Cramer, T. van der Sar, V. V. Dobrovitski, and R. Hanson, Nat. Nanotechnol. **9**, 171 (2014).
 - [10] C. Müller, X. Kong, J.-M. Cai, K. Melentijevic, A. Stacey, M. Markham, J. Isoya, S. Pezzagna, J. Meijer, J. Du, M.B. Plenio, B. Naydenov, L.P. McGuinness and F. Jelezko. Nat. Comm. **5**, 4703 (2014).
 - [11] J. Cai, F. Jelezko, M. B. Plenio, and A. Retzker, New J. Phys. **15**, 013020 (2013).
 - [12] A. Ajoy, U. Bissbort, M. D. Lukin, R. L. Walsworth, and P. Cappellaro, Phys. Rev. X **5**, 011001 (2015).
 - [13] M. Kost, J. Cai, and M. B. Plenio, Sci. Rep. **5**, 11007 (2015).
 - [14] G. Gordon, N. Erez, and G. Kurizki, J. Phys. B **40**, S75 (2007).

- [15] L. Cywiński, R. M. Lutchyn, C. P. Nave, and S. DasSarma, *Phys. Rev. B* **77**, 174509 (2008).
- [16] A. G. Kofman and G. Kurizki, *Phys. Rev. Lett.* **87**, 270405 (2001).
- [17] M. Biercuk, A. Doherty, and H. Uys, *J. Phys. B* **44**, 154002 (2011).
- [18] R. de Sousa, *Top. Appl. Phys.* **1150**, 183 (2009).
- [19] H. Y. Carr and E. M. Purcell, *Phys. Rev.* **94**, 630 (1954).
- [20] S. Meiboom and D. Gill, *Rev. Sci. Instrum.* **29**, 688 (1958).
- [21] A. A. Maudsley, *J. Magn. Reson.* **69**, 488 (1986).
- [22] T. Gullion, D. B. Baker, and M. S. Conradi, *J. Magn. Reson.* **89**, 479 (1990).
- [23] J.-M. Cai, B. Naydenov, R. Pfeiffer, L. P. McGuinness, K. D. Jahnke, F. Jelezko, M. B. Plenio, and A. Retzker, *New J. Phys.* **14** 113023 (2012).
- [24] A. Albrecht and M.B. Plenio, *Phys. Rev. A* **92**, 022340 (2015).
- [25] C. A. Ryan, J. S. Hodges, and D. G. Cory, *Phys. Rev. Lett.* **105**, 200402 (2010).
- [26] A. M. Souza, G. A. Alvarez, and D. Suter, *Phys. Rev. Lett.* **106**, 240501 (2011).
- [27] A. M. Souza, G. A. Alvarez, and D. Suter, *Phil. Trans. R. Soc. A* **370**, 4748 (2012).
- [28] D. Farfurnik, A. Jarmola, L. M. Pham, Z.-H. Wang, V. V. Dobrovitski, R. L. Walsworth, D. Budker, N. Bar-Gill, E-print arXiv:1505.00636.
- [29] N. Zhao, J. Wrachtrup, and R. -B. Liu, *Phys. Rev. A* **90**, 032319 (2014).
- [30] N. Zhao, Z.-Y. Wang, and R.-B. Liu, *Phys. Rev. Lett.* **106**, 217205 (2011).
- [31] P. Huang, X. Kong, N. Zhao, F. Shi, P. Wang, X. Rong, R.-B. Liu, and J. Du, *Nat. Commun.* **2**, 570 (2011).
- [32] M. Loretz, J. M. Boss, T. Rosskopf, H. J. Mamin, D. Rugar, and C. L. Degen, *Phys. Rev. X* **5**, 021009 (2015).
- [33] D. T. Gillespie, *Phys. Rev. E* **54**, 2084 (1996).
- [34] J. R. Maze, J. M. Taylor, and M. D. Lukin, *Phys. Rev. B* **78**, 094303 (2008).